Rutherford Backscattering Spectrometry analysis of iron-containing Bi2Se3 Topological Insulator thin films

Victor Alarcon-Diez, Mahmoud Eddrieff, Ian Vickridge

Rutherford Backscattering Spectrometry analysis of iron-containing Bi_2Se_3 Topological Insulator thin films

Alarcon-Diez, V.[1*], Eddrief, M.[1,2], Vickridge, I.[1,2]

[1]Sorbonne Universités, UPMC Univ Paris 06, UMR7588, INSP, F-75005, Paris, France

[2]CNRS, UMR7588, INSP, F-75005, Paris, France

Keywords: RBS, Topological insulators, Bi_2Se_3, Fe-Se intergrowth.

Abstract

Fe-containing Bi_2Se_3 Topological Insulators (TI) thin films have been grown to investigate the intricate interplay between topological order and the incorporation of ferromagnetic atoms. Here we present the quantitative characterisation of the Bi_2Se_3 thin films with up to 16 at% Fe incorporated during the growth process on GaAs (111) substrate by Molecular Beam Epitaxy. We report the elemental composition and depth profiles of the Bi_2Se_3:Fe films obtained using Rutherford Backscattering Spectrometry (RBS) and their formed crystalline phase obtained by X-Ray Diffraction (XRD). Resistance of the TI to beam-induced damage was investigated by channelling RBS. Using the elemental composition from RBS and the thickness from XRD measurements the Fe-free film density was deduced. For Fe-containing samples, the diffraction reveals the formation of two distinct crystalline phases, as well as their intergrowth pattern, in which the basal planes of Bi_2Se_3 coexist with an additional Fe-Se phase. This intergrown composite, with chemical compatibility of the Fe-Se phase with the crystalline Bi_2Se_3 structure, preserves the intrinsic topological surface states of the TI component despite the inhomogeneous distribution of the constituent phases. RBS analysis gives the stoichiometry of the Bi_2Se_3, and Bi_2Se_3:Fe samples (estimated between 0-16 atom% Fe) and gives insights into the composition of $FeSe_x$ phases present.

[*] Corresponding author Tel. : +33 1 44 27 46 88
E-mail address : victor.alarcon@insp.upmc.fr (V. Alarcon-Diez)

Introduction

In three-dimensional topological insulators (TIs), the strong intrinsic spin-orbit coupling generates an insulator band inversion with spin-momentum locking leading to creation of protected Topological Surface States (TSS) due to Time-Reversal (TR) symmetry [1]. These surface states are described by the relativistic Dirac Hamiltonian - Dirac cone - with massless Dirac fermions as charge carriers. The charge carriers are characterised by their helicity property and the topological order of their surface states, meaning that opposing electron spin states generate opposing currents without backscattering effects. These states are very robust under TR variations [2]. The topological nature with its spin texture is extremely interesting not only from the technological perspective, for example in quantum computing and spintronic devices, but also in fundamental particle physics (Majorana fermions, axions, magnetic monopoles…) [3]. However for such applications it is necessary to be able to form a ferromagnetic TSS, breaking TR symmetry and thus opening the Dirac cone and creating a band gap in the TSS. This may be attempted through doping with a magnetic dopant [4, 5], to give for example Bi_2Se_3:Fe. Bi_2Se_3 has been used due to the band structure, with just one Dirac cone in the TSS and the bulk energy band gap compatible with ambient temperature, together with a well-defined crystal structure.

In this work, we have quantitatively studied the elemental composition of Bi_2Se_3:Fe topological insulator thin films. The Bi_2Se_3 samples were epitaxially grown by Molecular Beam Epitaxy (MBE) on GaAs (111) substrates and including varying concentrations of Fe in the growth process to obtain Bi2Se3:Fe samples, with Fe/(Bi +Se +Fe) atomic ratios up to 16% (reported in Table 2 below). The films were 100 nm thick, either uncapped or capped to protect from oxidation. We will show that the Fe reacts with the Se, forming $FeSe_x$, this intergrowth compound having no influence on the topologic gapless surface state. Rutherford Backscattering Spectrometry (RBS) was applied to determine film elemental compositions and concentration depth profiles. To our knowledge, these are the first direct quantitative determinations of the elemental composition of such thin Bi_2Se_3:Fe films.

Methodology

The Bi_2Se_3 samples are grown by MBE on GaAs (111) substrate and either left uncapped or capped with one of three layers: ZnSe, Se or Au. More details of the epitaxy and characterization of the Fe-free Bi_2Se_3 films are given in [6]. For the RBS analysis presented here, Au capping was used in order to avoid overlapping the signals from the TI with that of the capping layer. Growth is conducted under Se-rich conditions – similar to the case of the GaAs buffer layer grown under As rich condition – since the substrate temperature during growth is greater than that at which Se (or As) evaporates. In the Bi2Se3:Fe samples, Fe was evaporated at the same time as the Bi and Se, with the nominal Fe content being controlled through the Fe flux, which was varied via the temperature (T_{Fe}) of the Fe Knudsen cell.

Elemental composition was obtained by Rutherford Backscattering Spectrometry (RBS) using an α^+ ion beam of energies between 1500 and 2000 keV, with 5-20 nA in a 0.5 to 1 mm beam spot. Under these conditions deadtime was less than 1% and pileup was negligible. The backscattering angle varied between 145° and 165°. X-Ray Diffraction (XRD) was also undertaken as a complementary technique, using monochromatic Cu Kα x-rays. The Bi_2Se_3 structure consists of a 5-layer unit cell dominated by covalent bonds, with the stack of 5-layer units (quintuple-layers, or QL) held together via van der Waals forces. Since the van der Waals forces are weak, we also investigated the stability under the analysis beam of the TI layers by channelling RBS.

The NDF DataFurnace code (NDFv9.6a and WiNDFv9.3.76) [7] was used to fit the RBS spectra. Spectra were taken at several points on each sample. All of the spectra from a given sample were fitted simultaneously with NDF in order to improve the statistics and increase the representivity of the studied area. SRIM-2003 stopping power was used [8]. We found it necessary to apply a correction of 0.9 to the stopping power of gallium in order to obtain adequate fits of the substrate plateau height. This correction produces the correct plateau height in a GaAs bulk sample. The Chu

model was used for the straggling [9], Andersen for screening [10] and Molodtsov and Gurbich for pile-up correction [11]. Double scattering was implemented in order to get good fits to the GaAs substrate signal at low energies [12] in the spectra. In all cases the detector dead layer (determined elsewhere) was included in the fit model.

Results and discussion

1. *He beam damage*

Possible beam damage was assessed from channelling spectra. The beam was aligned with the GaAs < 1 1 1 > axis, which corresponds to < 0 0 1 > in Bi_2Se_3, and aligned spectra were acquired for increasing incident beam charge. Angular scans showed that the Bi_2Se_3 < 0 0 1> axis was aligned with the GaAs < 1 1 1 > axis. Figure 1 shows the random spectrum, and a series of channelled spectra accumulated for increasing incident beam charge (expressed in ions/nm^2). The random spectra were obtained by summing several spectra obtained from pseudo-random orientations. The disorder in the lattice has been parameterized by the random/channelled ratio (chi, X) which is 0.23 in the Bi peak and 0.32 in Se at the lowest beam fluence. While in an ideal well-ordered crystal X would be less than 0.05, in these samples significantly larger disorder was observed. We also note higher X in the Se peak than in the Bi peak. Further channelling studies aimed at understanding this are underway, however this shows the robustness of the TI, since all the studied samples show TSS [6, 13] even with this degree of disorder. The damage evolves slightly with the deposited charge, as shown in Figure 2, where it is possible to observe a slight increase in X as the fluence increases from 31 ions/nm² (5 μC in 1 mm beam diameter) to 656 ions/nm^2 (105 μC). The fluence used for experiments reported here was never greater than 93 ion/nm^2 (15μC) and we conclude that beam damage may safely be neglected for these composition measurements, which are all obtained for random orientation of the samples.

2. Composition

In the case of uncapped layers, uncontrolled oxidation occurred, and in the case of Se and ZnSe capped layers, contributions to the spectrum from the capping layer contributed significant uncertainty to the estimation of the amount of Se in the TI layer itself. We present here only RBS results for three gold-capped Bi_2Se_3 layers, which gave the best analysis conditions for NDF Data Furnace. In sample 1, no Fe was introduced during the growth. In samples 2 and 3, Fe was evaporated at temperatures T_{Fe} of 1360°C and 1370°C respectively during growth.

In all cases, spectra from several points and/or measured at different angles and incident beam energies were simultaneously fitted with NDF, yielding areal densities for Fe, Bi and Se, as shown in Figure 3. Once the optimum fit was obtained, the uncertainty for each fit was assessed by re-fitting the spectra with the Bi/Se ratio and Fe content constrained to a desired value (leaving NDF free to optimise charge, gain, detector angle etc, as was the case for the unconstrained fitting). Goodness of fit was then judged by eye and the range of Bi/Se ratios and Fe content consistent with the data was judged from the range of these constrained fits that were consistent with the data. An example of such a series of constrained fits is given in Figure 4. Note that these uncertainties are only those associated with the fitting process and the information contained in the spectra: systematic uncertainties (e.g. uncertainties in screening corrections or stopping powers) are not considered, but will be common to all measurements.

The summary of the fitted results and range of values found is given in Table 1.

We first note that in all cases the films are rich in selenium, since in stoichiometric Bi_2Se_3 Bi/Se would be 0.67. Careful attention was paid to obtaining good random spectra so that undesired channelling effects are negligible here. The MBE is undertaken under Se-rich conditions, however the films have well-defined X-Ray diffraction peaks for undistorted Bi_2Se_3 (blue line in Figure 6) and no local perturbations are observed by Transmission Electron Microscopy (TEM, not shown here). This implies that any excess selenium is in sites that do not disturb the lattice structure. The Fe-free film displays

the expected TSS behaviour and the Dirac cones are observed in ARPES [6, 13] so the selenium excess is not having a significant effect on these properties of the system either. Similar composition has been found in uncapped samples and samples with different capping layers, always obtaining an excess of Se although with greater uncertainties as mentioned above. We note that the RBS spectra indicate homogeneous concentration with depth, which is shown in Figure 5 for the Bi_2Se_3 sample. RBS spectra from the Bi_2Se_3:Fe samples also indicate constant composition with depth, including for the Fe for which a signal is also visible in the spectra.

We can reformulate the compound as $Bi_2Se_3 + Se_{excess}$. For the Fe-free sample Se_{excess} is 11±3% of the total amount of Se. This surprising result will require further characterisation in order to understand where the excess Se is, however this result is consistent with the channelling spectra obtained during the beam damage investigation. The Bi channelling yield is about 23% of that of the random yield whilst the Se channelling yield is about 32%. If the sample were to be just disordered Bi_2Se_3 we might expect to have similar disorder in the two sublattices, with Se also having a channelling yield around 23%. It is intriguing that the Se channelling yield is equal to that of the Bi plus 9% more of the total Se yield – close to the 11% overall Se excess observed in random RBS spectra.

The small difference in temperature for the Fe Knudsen cell between samples 2 and 3 corresponds to 8 % difference in Fe vapour pressure [14] and thus Fe flux arriving at the growth surface, which is consistent with the difference in Fe concentration observed. Finally, we note that as the Fe content increases, the Bi/Se ratio decreases. This suggests the possible presence of Fe-Se phases, which we denote $FeSe_x$. The Fe-Se phase diagram is complex [15] however XRD of Fe-rich films shows peaks consistent with $FeSe_x$ phases (orange and green lines in Figure 6). Due to the complexity of the phase diagram and the associated complexity in indexing the XRD peaks we cannot know with certainty the number and identity of all the phases, since it is not possible to index them all using ordinary methods. We noted that the primary pattern is from Bi_2Se_3, whose expected Bragg peak positions are marked with ticks – (0 0 *l*) reflections, which obey the rhombohedral diffraction condition *l* = 3n,

while the indexation of $FeSe_x$ phase peaks remains yet to be determined. However substantial disorder has been found in Bi_2Se_3:Fe samples since the Bi_2Se_3 Bragg peaks are broader for these samples than those obtained from the Fe-free sample. Furthermore, the Fe-Se alloy peak positions are the same between the two samples, indicating that in the two samples the basal planes of the $FeSe_x$ phases have the same alignment with respect to the Bi_2Se_3 planes. Nevertheless the $FeSe_x$ planes are probably different due to an inhomogeneous distribution with different texture orientations. The XRD measurements also gave a measure of the physical thickness of the Fe-free film, through the Laue oscillations observed in the wings of the Bi_2Se_3 Bragg peaks.

Under this scenario it is possible to consider the quantity of Se as the sum of three different contributions: that related to Bi forming Bi_2Se_3 (Se_{Bi}), that in excess Se_{excess}, and that forming an alloy $FeSe_x$ (Se_{Fe}) so that we consider the film to be composed of Bi_2Se_3 + Se_{excess} + $FeSe_x$. Furthermore, Angle-resolved PhotoEmission spectrometry (ARPES) measurements (not shown here) on these Fe-rich samples show that the Dirac cone has not been opened, suggesting that there is little or no Fe substitution into the Bi_2Se_3 lattice. Although the Fe-Se phases are not yet known, the results found by RBS can be used to calculate the overall index *x* for this alloy, as the Se/Fe ratio. This calculation has been based on the formulation Bi_2Se_3 + Se_{excess} + $FeSe_x$ and the results extracted by NDF fits with all the conceivable values of x, taking several possible values for Bi/Se_T (where $Se_T = Se_{Bi} + Se_{excess} + Se_{Fe}$) and the Fe content, within the uncertainty limits, and averaging them to find the best estimate for *x*. Two extreme hypotheses are presented in Table 2. At one extreme, we assume that the percentage Se excess in the Bi_2Se_3:Fe samples is the same as that experimentally determined in the Bi_2Se_3 sample (Se_{excess} = 11%). At the other extreme, we assume that all excess Se is associated with $FeSe_x$ phases (Se_{excess}= 0). In both cases, $x < 1$ (Fe-rich) for T_{Fe} =1360°C, and $x > 1$ (Se-rich) for T_{Fe}=1370°C. The resulting estimates of the atomic percentage of $FeSe_x$ in Fe rich samples are 21 % for sample 2 and 33 % for sample 3 when Se_{excess} = 11 % (experimental value reported above for the Bi_2Se_3 film) and 27 % and 39 % when a perfect stoichiometry of Bi_2Se_3 is assumed (Se_{excess}= 0).

Furthermore the atomic and mass densities for the Bi_2Se_3 iron free sample can be calculated from the number of atoms and physical thickness obtained in RBS and XRD respectively. We find ρ_{atomic} = (3.88 ± 0.15) · 10^{22} cm^{-3} and ρ_{mass}= 8.22 ± 0.32 g·cm^{-3}, when taking into account the total number of atoms measured (Bi_2Se_3 + Se_{excess}). On the other hand, if we just count the number of Se atoms that would be required to form stoichiometric Bi_2Se_3 and ignore Se_{excess}, we obtain ρ_{atomic} = (3.62 ± 0.18) · 10^{22} cm^{-3} and ρ_{mass}= 7.88 ± 0.39 g·cm^{-3}. The first result is significantly greater than the expected density for an ideal Bi_2Se_3 crystal which may be calculated from the unit cell, giving 3.55·10^{22} cm^{-3} and 7.71 g·cm^{-3} atomic and mass density respectively, whereas the second result is in good agreement, further underlining the view that the excess Se is present in such a way as to not disturb the Bi_2Se_3 lattice.

Conclusions

RBS-channelling showed that the Bi_2Se_3 layers are sufficiently robust to allow RBS analysis without significant beam induced damage. The initial amount of disorder, with the smallest value of X observed to be 0.23, is significantly greater than that expected for a defect-free crystal.

The elemental composition extracted by RBS in combination with XRD of the Bi_2Se_3 films, shows an excess in Se (Se_{excess}) of 11±3%, which we describe as Bi_2Se_3 + Se_{excess}. Nevertheless neither the lattice structure measured by XRD nor the electronic properties are different from those expected for an ideal Bi_2Se_3 TI. Moreover the density calculations also suggest that the Se excess does not significantly disrupt the Bi_2Se_3 structure. Bi_2Se_3:Fe samples show a decreasing Bi/Se ratio as a function of the amount of incorporated Fe. The presence of Fe-Se phases is shown by XRD spectra and the great majority of Fe atoms are within this $FeSe_x$ alloy, hence Fe atoms are probably not diluted within Bi_2Se_3. The alloy has been expressed as $FeSe_x$, where *x* is Se/Fe ratio. Whatever hypothesis is retained for the distribution of the Se not incorporated into stoichiometric Bi_2Se_3, the composition determined by RBS allows us to deduce that overall the $FeSe_x$ phases are Fe-rich (x<1) for sample 2 (T_{Fe}= 1360°C) and Se-rich (x>1) for sample 3 (T_{Fe}=1380°C).

Further experiments are planned using other Ion Beam Analysis (IBA) techniques, such as Particle Induce X-ray Emission (PIXE), in order to study samples with smaller Fe concentrations, and using a large solid angle segmented detector in order to reduce uncertainty through improved statistics. Since such a detector will also produce spectra for a range of detection angles, this will also reduce the mass/depth ambiguity in samples capped with Se or ZnSe, allowing more meaningful composition studies to be performed by RBS with such samples. Channelling studies of Bi_2Se_3 and Bi_2Se_3:Fe films are also likely to shed further light on the nature of the disorder in the films and could provide further clues about the nature of the excess Se.

Acknowledgements

This work has been supported by Marie Curie Actions - Initial Training Networks (ITN) as an Integrating Activity Supporting Postgraduate Research with Internships in Industry and Training Excellence (SPRITE) under EC contract no. 317169. We are very grateful to the ALTAÏS accelerator team from Namur University in Belgium, where the IBA experiments took place, and to Emrick Briand and Sebastien Steydli of INSP for efficient technical assistance with the RBS measurements. We are also very grateful to Sarah Hidki of INSP, for the excellent XRD experiments.

Bibliography

[1] L. Fu, C. L. Kane, and E. J. Mele, "Topological insulators in three dimensions," *Phys. Rev. Lett.*, vol. 98, no. March, pp. 1–4, 2007.

[2] M. Z. Hasan and C. L. Kane, "Colloquium: Topological insulators," *Rev. Mod. Phys.*, vol. 82, no. 4, pp. 3045–3067, Nov. 2010.

[3] L. A. Wray, "Device Physics: Topological transistor," *Nat. Phys.*, vol. 8, no. 10, pp. 705–706, 2012.

[4] Q. Liu, C.-X. Liu, C. Xu, X.-L. Qi, and S.-C. Zhang, "Magnetic Impurities on the Surface of a Topological Insulator," *Phys. Rev. Lett.*, vol. 102, no. 15, p. 156603, Apr. 2009.

[5] J.-M. Zhang, W. Zhu, Y. Zhang, D. Xiao, and Y. Yao, "Tailoring Magnetic Doping in the Topological Insulator Bi_{2}Se_{3}," *Phys. Rev. Lett.*, vol. 109, no. 26, p. 266405, Dec. 2012.

[6] M. Eddrief, P. Atkinson, V. Etgens, and B. Jusserand, “Low-temperature Raman fingerprints for few-quintuple layer topological insulator Bi2Se3 films epitaxied on GaAs.,” *Nanotechnology*, vol. 25, no. 24, p. 245701, Jun. 2014.

[7] N. P. Barradas and C. Jeynes, “Advanced physics and algorithms in the IBA DataFurnace,” *Nucl. Instruments Methods Phys. Res. Sect. B Beam Interact. with Mater. Atoms*, vol. 266, no. 8, pp. 1875–1879, Apr. 2008.

[8] J. F. Ziegler, “SRIM-2003,” *Nucl. Instruments Methods Phys. Res. Sect. B Beam Interact. with Mater. Atoms*, vol. 219–220, pp. 1027–1036, Jun. 2004.

[9] W. K. Chu, “Calculation of energy straggling for protons and helium ions,” *Phys. Rev. A*, vol. 13, no. 6, pp. 2057–2060, Jun. 1976.

[10] H. H. Andersen, F. Besenbacher, P. Loftager, and W. Möller, “Large-angle scattering of light ions in the weakly screened Rutherford region,” *Phys. Rev. A*, vol. 21, no. 6, pp. 1891–1901, Jun. 1980.

[11] S. L. Molodtsov and A. F. Gurbich, “Simulation of the pulse pile-up effect on the pulse-height spectrum,” *Nucl. Instruments Methods Phys. Res. Sect. B Beam Interact. with Mater. Atoms*, vol. 267, no. 20, pp. 3484–3487, Oct. 2009.

[12] N. P. Barradas, “Double scattering in grazing angle Rutherford backscattering spectra,” *Nucl. Instruments Methods Phys. Res. Sect. B Beam Interact. with Mater. Atoms*, vol. 225, no. 3, pp. 318–330, Sep. 2004.

[13] F. Vidal, M. Eddrief, B. Rache Salles, I. Vobornik, E. Velez-Fort, G. Panaccione, and M. Marangolo, “Photon energy dependence of circular dichroism in angle-resolved photoemission spectroscopy of Bi 2 Se 3 Dirac states,” *Phys. Rev. B*, vol. 88, no. 24, p. 241410, Dec. 2013.

[14] D. R. Lide, *CRC Handbook of Chemistry and Physics, 84th Edition*. 2003, CRC Press, ISBN 9780849304842

[15] H. Okamoto, “The FeSe (Iron-Selenium) system,” *J. Phase Equilibria*, vol. 12, no. 3, pp. 383–389, Jun. 1991.

List of Tables

Table 1

	Bi/Se	Fe (%)	Thickness (TFU)	Thickness (nm)
Sample 1 (no Fe)	0.59±0.02	0	489±3	137.7±0.9
Sample 2 (T_{Fe} 1360°C)	0.51±0.03	14±2	295±5	83.1±1.4
Sample 3 (T_{Fe} 1370°C)	0.43±0.02	16±2	472±3	133.0±0.9

Table2

			***x*=Se/Fe**	
	Bi/Se	**Se_{excess}/Se_T**	**Sample 2**	**Sample 3**
Experimental fitting	0.59	0.11	0.51±0.15	1.02±0.23
Stoichiometry	0.67	0	0.94±0.19	1.32±0.26

List of Figures

Figure 1

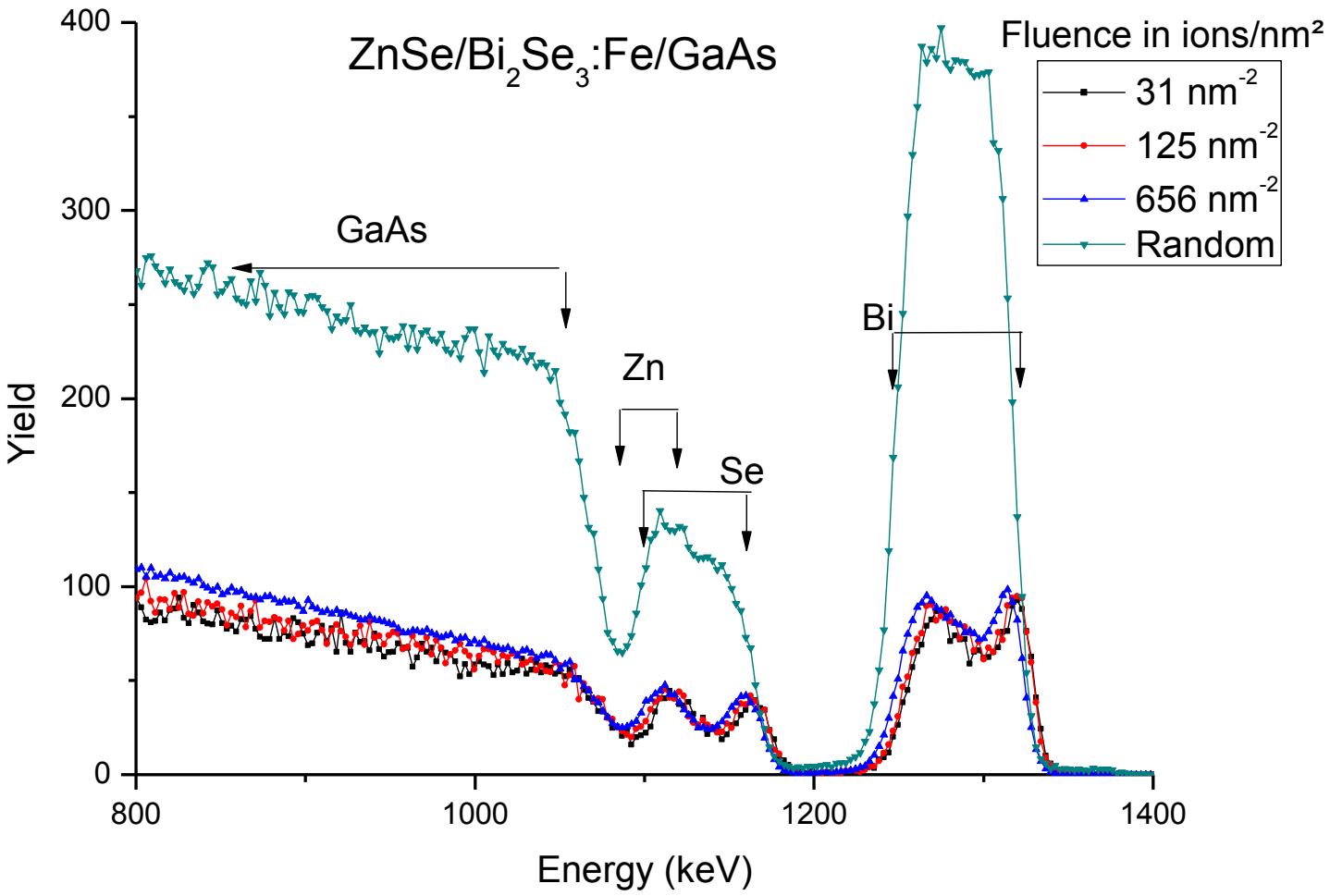
ZnSe/Bi2Se3:Fe/GaAs
Fluence in ions/nm²
31 nm-2
125 nm-2
656 nm-2
Random
GaAs
Zn
Se
Bi
Yield
Energy (keV)
0
100
200
300
400
800
1000
1200
1400

Figure 2

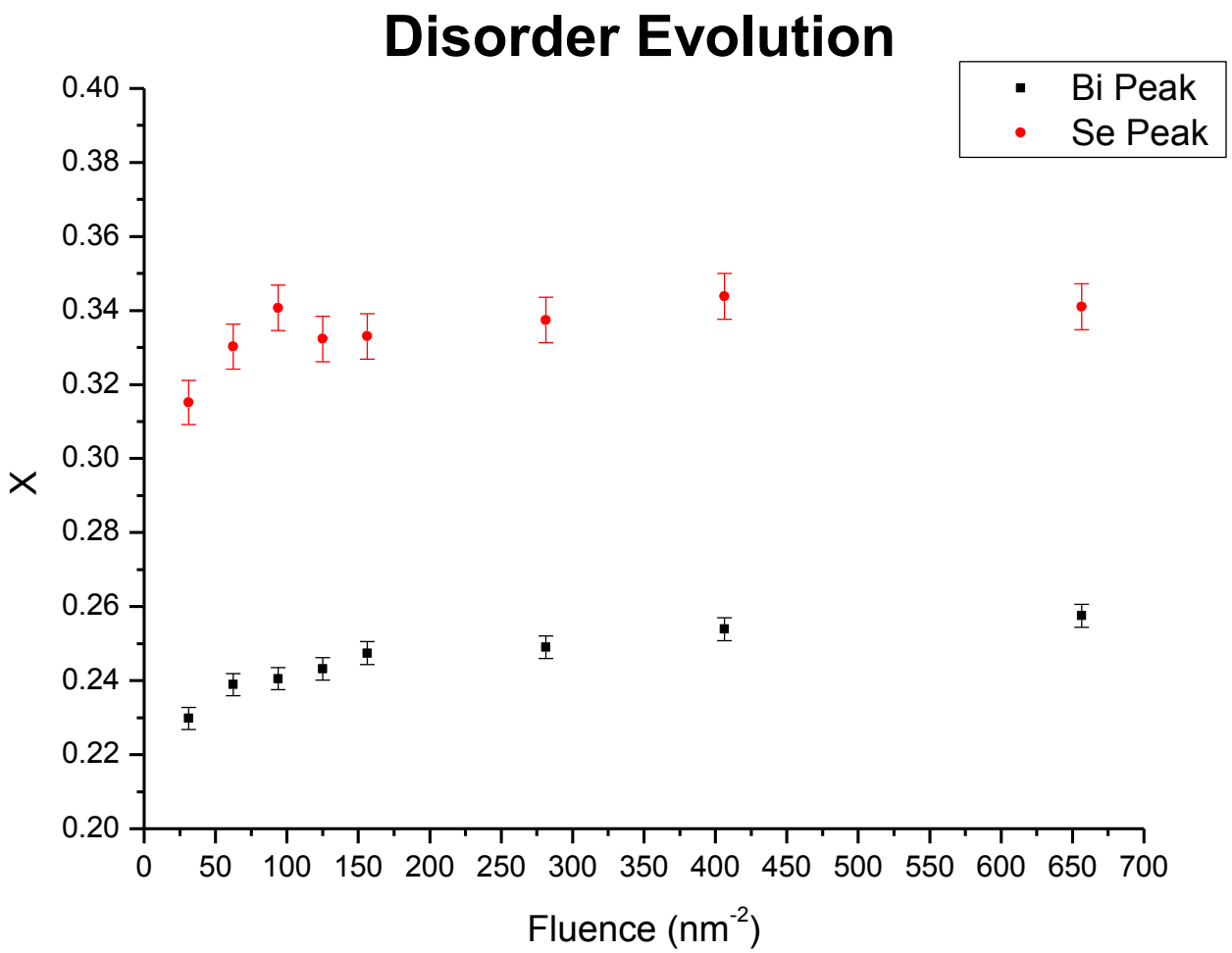
Disorder Evolution
Bi Peak
Se Peak
X
0.40
0.38
0.36
0.34
0.32
0.30
0.28
0.26
0.24
0.22
0.20
0
50
100
150
200
250
300
350
400
450
500
550
600
650
700
Fluence (nm-2)

Figure 3

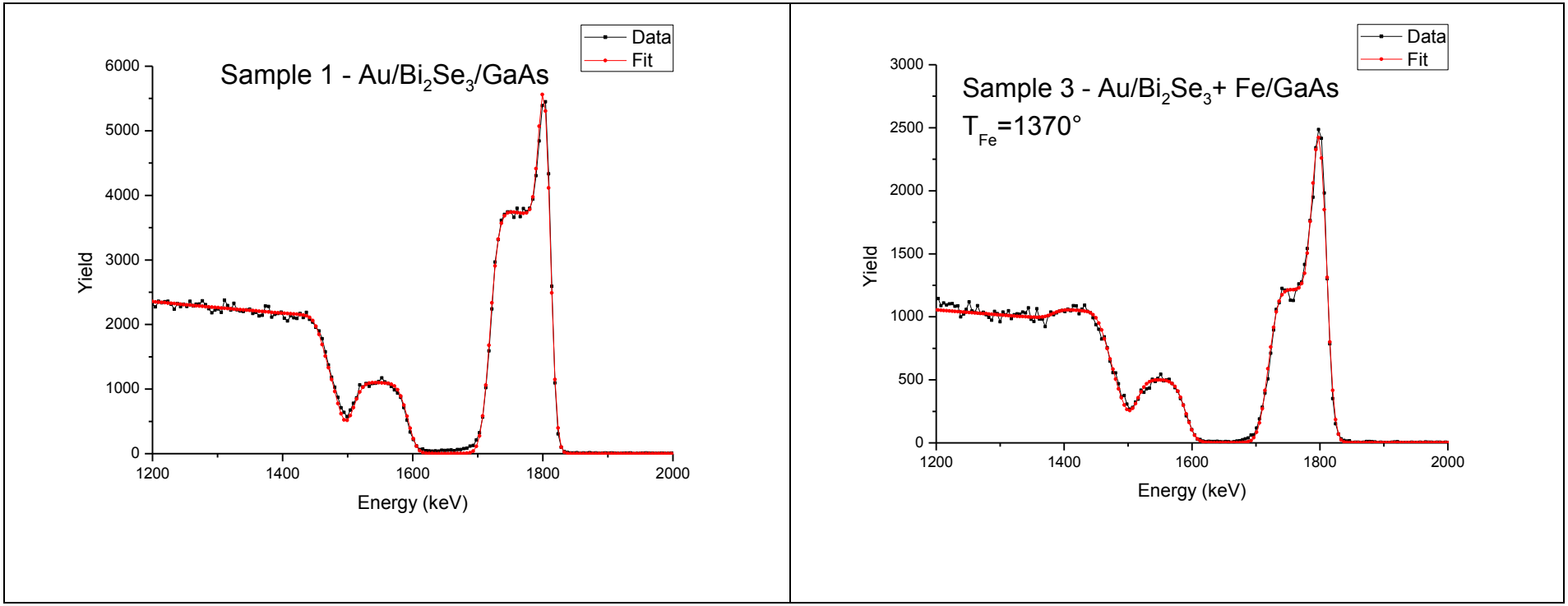
Sample 1 - Au/Bi2Se3/GaAs
Data
Fit
Yield
Energy (keV)
0
1000
2000
3000
4000
5000
6000
1200
1400
1600
1800
2000
Sample 3 - Au/Bi2Se3+ Fe/GaAs
TFe=1370°
Data
Fit
Yield
Energy (keV)
0
500
1000
1500
2000
2500
3000
1200
1400
1600
1800
2000

Figure 4

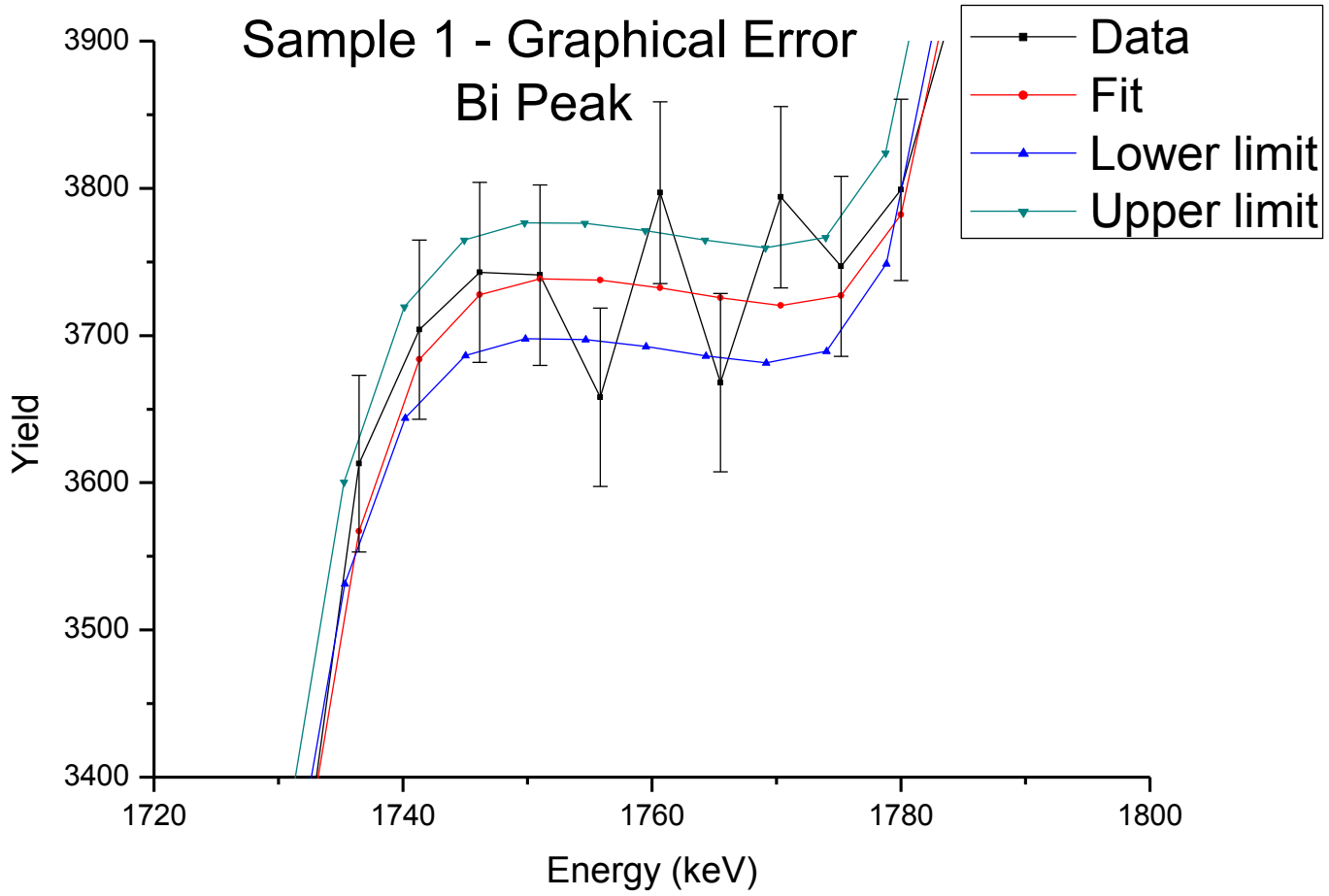
Sample 1 - Graphical Error
Bi Peak
Data
Fit
Lower limit
Upper limit
Yield
3900
3800
3700
3600
3500
3400
1720
1740
1760
1780
1800
Energy (keV)

Figure 5

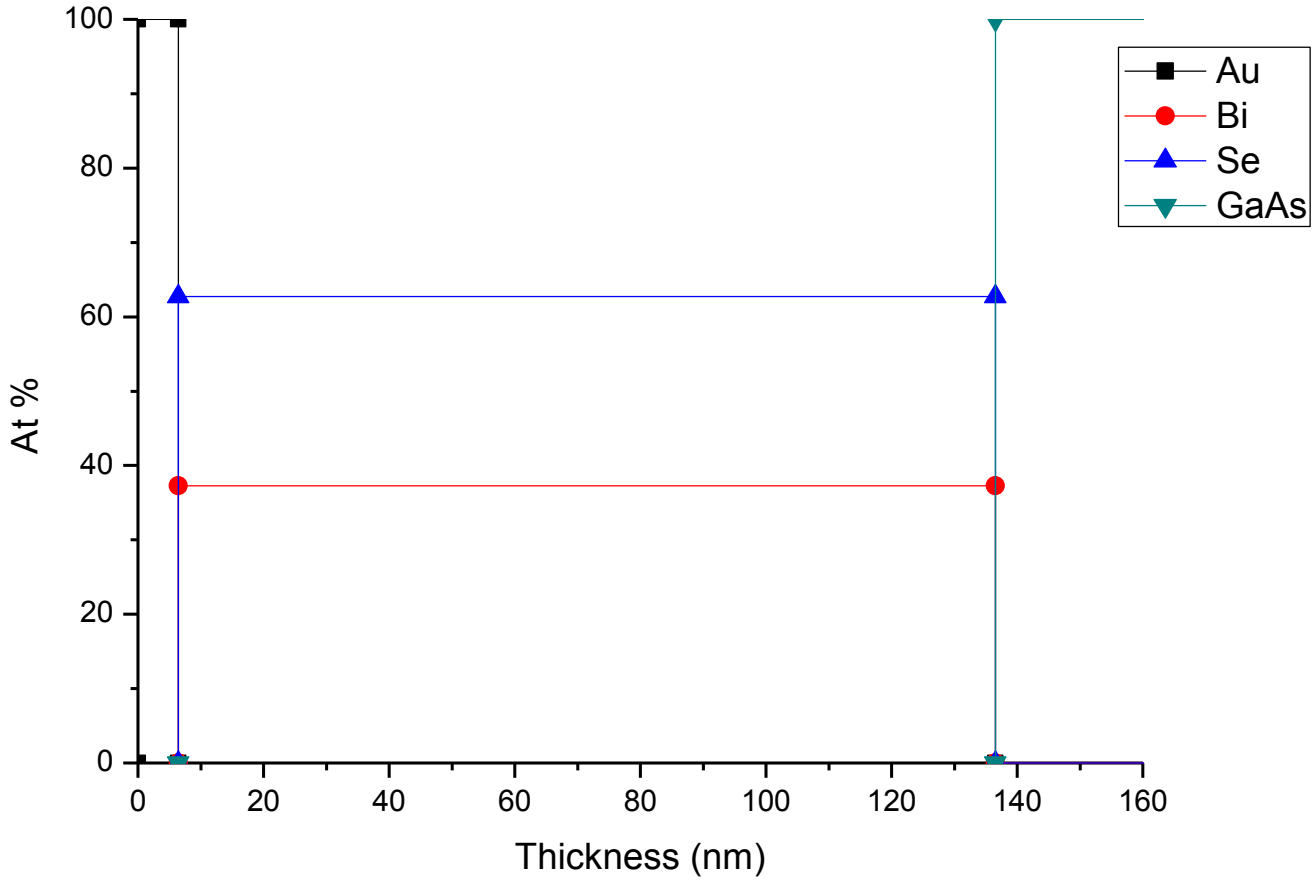
100
80
60
40
20
0
At %
0
20
40
60
80
100
120
140
160
Thickness (nm)
Au
Bi
Se
GaAs

Figure 6

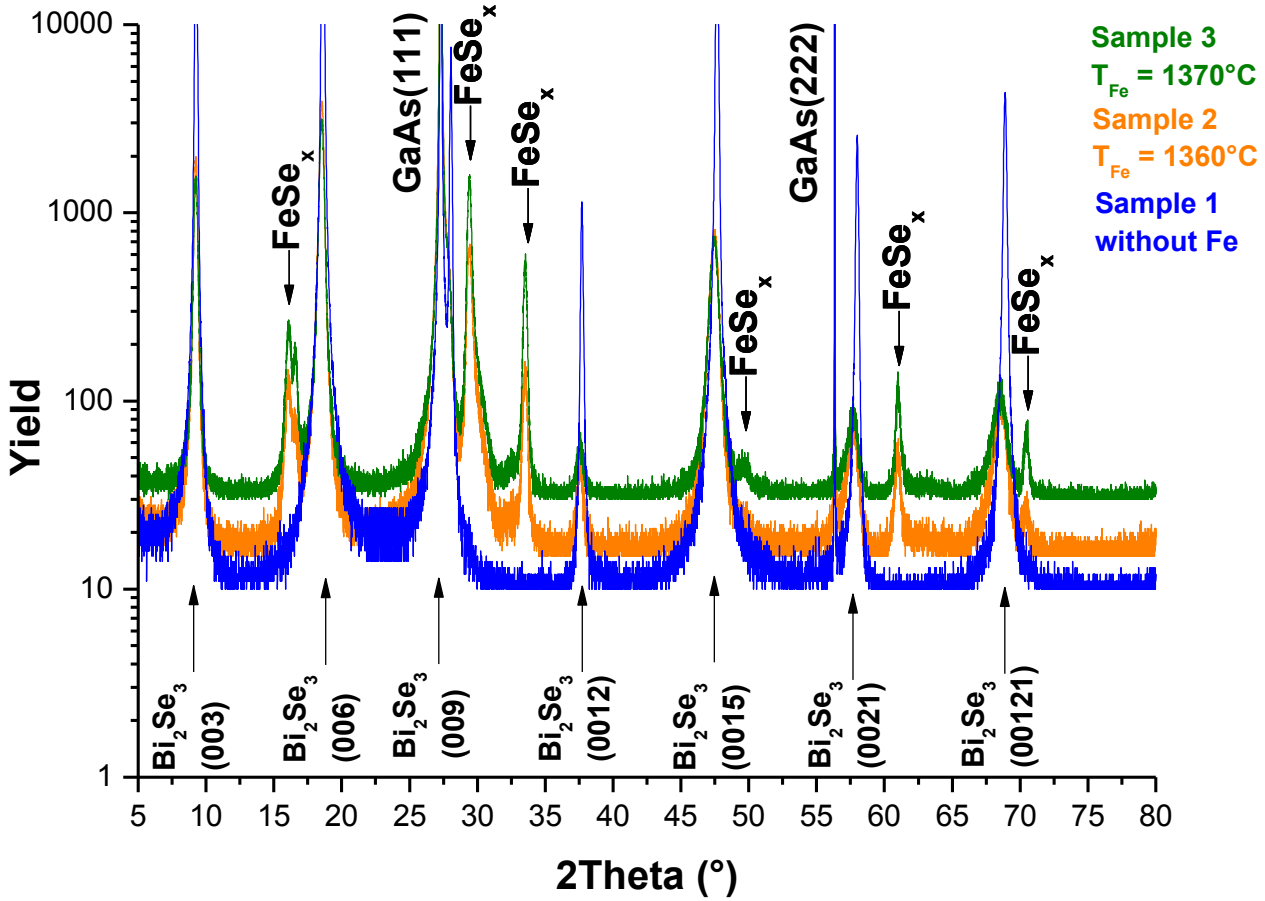
Yield
2Theta (°)
Sample 3
T_Fe = 1370°C
Sample 2
T_Fe = 1360°C
Sample 1
without Fe
FeSe_x
GaAs(111)
GaAs(222)
Bi2Se3 (003)
Bi2Se3 (006)
Bi2Se3 (009)
Bi2Se3 (0012)
Bi2Se3 (0015)
Bi2Se3 (0021)
Bi2Se3 (00121)